

LHC di-lepton searches for Z' bosons which explain measurements of $b \rightarrow sl^+l^-$ transitions

Ben Allanach^a

^a*DAMTP, University of Cambridge, Centre for Mathematical Sciences, Wilberforce Road, CB3 0WA, Cambridge, United Kingdom*

Abstract

Several current measurements of $b \rightarrow sl^+l^-$ processes are in tension with Standard Model predictions, whereas others (e.g. R_K and R_{K^*}) are in reasonable agreement with them. We examine some recent Z' models that fit the data as a whole appreciably better than does the Standard Model, confronting the models with ATLAS resonance searches in the e^+e^- and $\mu^+\mu^-$ channels. Both channels constrain the models; we find that the searches rule out less than one fifth of the allowed range of $M_{Z'}$. We estimate that the HL-LHC can roughly double the current sensitivity in $M_{Z'}$, but covering the whole parameter space would take a more powerful machine, such as a 100 TeV pp collider.

Some experimental measurements of B -meson decays involving the $b \rightarrow sl^+l^-$ transition are in tension with Standard Model (SM) predictions [1]. Focusing on the most discrepant measurements, the branching ratio $BR(B_s \rightarrow \phi\mu^+\mu^-)$, for example, is measured [2] to be 4σ below SM predictions. Some angular distributions in $B \rightarrow K^*\mu^+\mu^-$ decays are also around 4σ [3, 4, 5], as is $BR(B \rightarrow K\mu^+\mu^-)$ [6]. On the other hand, many other measurements involving the $b \rightarrow sl^+l^-$ transition are compatible with SM predictions, notably R_K and R_{K^*} , which are ratios of branching ratios

$$R_M = \frac{BR(B \rightarrow M\mu^+\mu^-)}{BR(B \rightarrow Me^+e^-)},$$

for $M \in \{K, K^*\}$ [7]. Although the aforementioned more discrepant observables do suffer larger theoretical errors, several estimates (e.g. Refs. [1, 6])

Email address: `ben.allanach.work@gmail.com` (Ben Allanach)

imply that theoretical uncertainties are insufficient to explain the tensions whilst respecting other measurements.

In Ref. [8], the SM was extended in order to ameliorate the tensions. An additional spontaneously broken $U(1)_X$ gauge group with family-dependent charges is posited to be in a direct product with the SM gauge group. The resulting additional TeV-scale vector boson, dubbed a Z' boson, mediates $b \rightarrow sl^{+l^-}$ transitions, altering predictions for their observables. The $U(1)_X$ charge assignment of the SM fermionic fields (including three right-handed fields) is

$$X = 3B_3 - (X_e L_e + X_\mu L_\mu + [3 - X_e - X_\mu] L_\tau), \quad (1)$$

where B_3 is third-family baryon number, L_e, L_μ and L_τ are first, second and third family lepton number, respectively and $X_e, X_\mu \in \mathbb{Q}$. These simple bottom-up models [8] explain why $|V_{td}|$, $|V_{ts}|$, $|V_{ub}|$ and $|V_{cb}|$ are all small compared to unity and why charged lepton flavour violation is suppressed. The assignment (1) is free of perturbative gauge anomalies, a necessary condition for a consistent theory. Previously, when it was thought that R_K and R_{K^*} differed more significantly from their SM predictions than updated analyses suggest, a Z' model with $X_\mu = 3$, $X_e = 0$ was proposed [9, 10, 11]. The case $X_e = X_\mu = X_\tau = 1$ was examined [12] more recently.

In a global fit to 247 measurements of processes involving the $b \rightarrow s$ transition and 148 LEP-2 e^+e^- to di-lepton data, Ref. [8] showed that the $U(1)_X$ models could provide a better fit than the SM by some 16 units of χ^2 and a reasonable goodness-of-fit with a p -value around 0.2 – 0.3. The fit is sensitive to the ratio of the Z' gauge coupling to the Z' mass $x := g_{Z'}/M_{Z'}$, X_e , X_μ and θ_{sb} , a mixing angle between s_L and b_L . For each value of X_e and X_μ , a fit was performed to x and θ_{sb} . It was found, assuming the hypothesis of the line of models parameterised by X_e/X_μ , that $-0.4 \leq X_e/X_\mu \leq 1.3$ to 95% confidence level (CL). We show the best-fit values of parameters from the fit as a function of X_e/X_μ in Fig. 1, for $X_\mu = 10$: these we shall use throughout the rest of this letter. The parameters are shown for $M_{Z'} = 3$ TeV and $X_\mu = 10$, although it is indicated on the left-hand ordinate of Fig. 1a how (to a good approximation) the best-fit gauge coupling scales¹ as a function of $M_{Z'}$.

Here for the first time, we re-cast direct Z' search results in this line

¹This scaling comes from the fact that all dimension-6 SMEFT operators induced by integrating out the Z' boson are proportional to $g_{Z'}^2/M_{Z'}^2$.

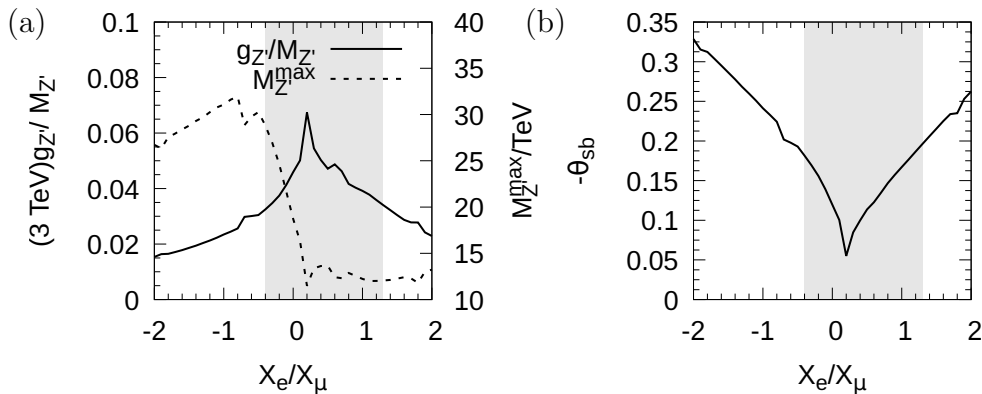


Figure 1: Best-fit model parameters along the model line parameterised by X_e/X_μ from the fit to flavour and LEP data in Ref. [8], for $X_\mu = 10$ and $M_{Z'} = 3$ TeV. The 95% CL region favoured by the fit is shaded. $M_{Z'}^{\text{max}}$ is an estimate of the maximum value of $M_{Z'}$ coming from perturbativity, explained just under (4).

of models. Such searches at the LHC have so far reported no significant excess and so we expect there to be concomitant constraints impinging on the parameter space of each model along the model line. We shall also provide rough sensitivity estimates for the high luminosity (HL-LHC) run for such searches.

In the models investigated here, the dominant production mode² of the Z' boson in pp collisions at the LHC is via $b\bar{b} \rightarrow Z'$ and thus the Z' production cross-section σ is suppressed by the small bottom parton distribution function squared, but otherwise

$$\sigma \propto g_{Z'}^2 \cos^4 \theta_{sb} = g_{Z'}^2 (1 - 2\theta_{sb}^2 + \mathcal{O}(\theta_{sb}^4)). \quad (2)$$

The production cross-section is therefore approximately independent of θ_{sb} if its value is significantly smaller than unity (this is the case for our model line) and indeed we shall neglect the dependence³ of θ_{sb} upon $M_{Z'}$.

A Z' decays into a fermion and an anti-fermion, to a good approximation. The partial width of a Z' boson decaying into a Weyl fermion f_i and a Weyl

²The next largest production mode production cross-section $(s\bar{b} + \bar{b}s) \rightarrow Z'$ is smaller than that of the $b\bar{b}$ production by a factor which depends on parameters, but is here always more than 20.

³We have checked that setting $\theta_{sb} = 0$ throughout instead makes scant difference to our results.

ij	$b\bar{b}$	$t\bar{t}$	e^+e^-	$\mu^+\mu^-$	$\tau^+\tau^-$	$\nu_e\bar{\nu}_e$	$\nu_\mu\bar{\nu}_\mu$	$\nu_\tau\bar{\nu}_\tau$
$\frac{\Gamma_{ij}}{M_{Z'}g_{Z'}^2\pi}$	$\frac{1}{4}$	$\frac{1}{4}$	$\frac{X_e^2}{12}$	$\frac{X_\mu^2}{12}$	$\frac{(3-X_e-X_\mu)^2}{12}$	$\frac{X_e^2}{24}$	$\frac{X_\mu^2}{24}$	$\frac{(3-X_e-X_\mu)^2}{24}$

Table 1: Partial widths of the Z' into various fermion/anti-fermion pairs in the massless unmixed fermion approximation.

anti-fermion \bar{f}_j is

$$\Gamma_{ij} = \frac{C}{24\pi} |g_{ij}|^2 M_{Z'}, \quad (3)$$

where g_{ij} is the coupling of the Z' boson to $f_i\bar{f}_j$ and C is the number of colour degrees of freedom of the fermions (here, 3 or 1). In the limit that $M_{Z'} \gg 2m_t$, we may approximate all fermions as being massless, save for the right-handed neutrinos, which we assume are more massive than $M_{Z'}/2$ and so are kinematically impossible for an on-shell Z' to decay into. We also neglect the small effects in decay widths coming from quark mixing. We show the various partial widths as functions of X_e and X_μ in Table 1. Summing all of these, we obtain a total Z' width of

$$\Gamma = \frac{4 + X_e^2 + X_\mu^2 + (3 - X_e - X_\mu)^2}{8\pi} g_{Z'}^2 M_{Z'}. \quad (4)$$

Perturbativity requires that the Z' is not too broad a resonance (here, we use $\Gamma/M_{Z'} < \frac{1}{2}$), yielding an upper limit upon $g_{Z'}$ from (4). Substituting this value into $g_{Z'}/M_{Z'}$ from Fig. 1a then yields a maximum value (which we call $M_{Z'}^{\max}$) of $M_{Z'}$ that can still provide a best-fit to the flavour and LEP data while maintaining perturbativity, as shown in Fig. 1a.

We display the values of some branching ratios into visible final-state particles in Fig. 2a for the case $X_\mu = 10$. We see from the figure that $\mu^+\mu^-$ and/or e^+e^- final states have an appreciable branching ratio. The LHC experiments perform searches in these by looking for a signal peak on top of a smooth background distribution in the di-lepton mass. Experimentally, di-leptons enjoy much higher efficiencies and/or lower backgrounds than $t\bar{t}$, $b\bar{b}$ or $\tau^+\tau^-$ and so we expect the $\mu^+\mu^-$ and e^+e^- channels to provide the best sensitivity, since there is no huge branching ratio factor favouring the other ones. From now on, we take ‘di-lepton’ states to mean $\mu^+\mu^-$ and e^+e^- .

In Ref. [13], ATLAS reported a search for heavy resonances in di-lepton invariant mass distributions for 139 fb^{-1} of 13 TeV pp collisions at the LHC.

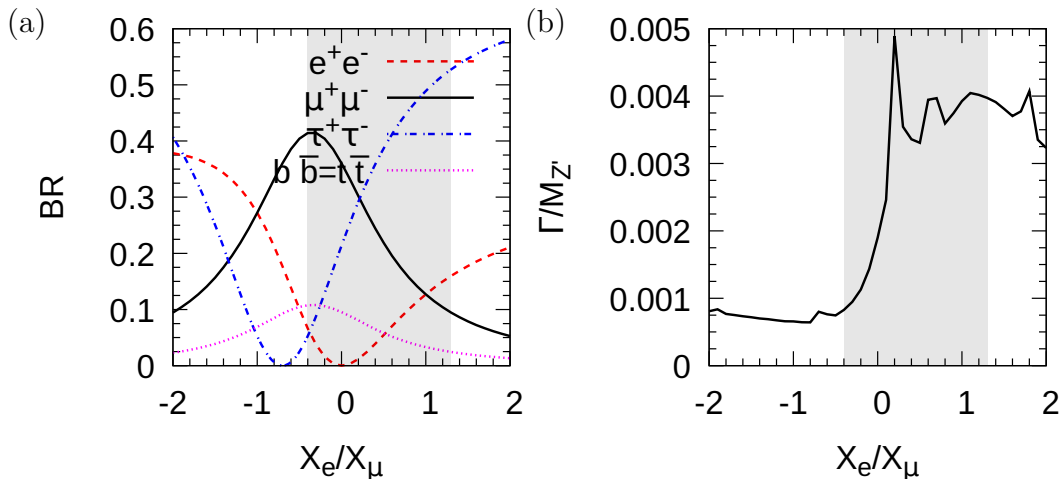


Figure 2: Z' decays for $M_{Z'} \gg 2m_t$ and $X_\mu = 10$ resulting from the fit to flavour and LEP-2 data in Ref. [8]: (a) predicted Z' branching ratios into observable final states. (b) width over mass for $M_{Z'} = 3$ TeV. The 95% CL region favoured by the fit is shaded.

Having observed no significant excess, ATLAS provides a 95% CL upper bound on production cross section multiplied by branching ratio of a new physics state decaying into the relevant di-lepton final state depending upon z , defined to be the ratio of the total width of the new physics state divided by its mass. We call this bound $s(z, M_{Z'})$. ATLAS provides bounds both for a narrow resonance ($s(0, M_{Z'})$) and for a resonance whose width is a tenth of its mass ($s(0.1, M_{Z'})$), as well as some particular discrete values of $z \in (0, 0.1)$. In Ref. [14], it was shown that for the di-muon final state, the function

$$s(z, M_{Z'}) = s(0, M_{Z'}) \left(\frac{s(0.1, M_{Z'})}{s(0, M_{Z'})} \right)^{\frac{z}{0.1}} \quad (5)$$

provides a reasonable interpolation for the bounds at other values of z between 0 and 0.1. We shall use (5) for the di-muon channel and also extend its use to the di-electron channel. As Fig. 2b shows, for the parameter set taken here ($X_\mu = 10$), the Z' boson is narrow for $M_{Z'} = 3$ TeV. In Fig. 3a, we validate (5) with data provided by the ATLAS collaboration at $z = 0.012$. The proximity of the dashed and solid curves in the figure demonstrates that the interpolation (5) also works for the e^+e^- channel. We compute the production cross-section times branching ratio at tree-level order with MadGraph3.5.3 [15], having encoded the model in UFO format [16].

We shall provide a rough and conservative estimate of the sensitivity of the HL-LHC di-lepton searches. We assume an integrated luminosity of 3000

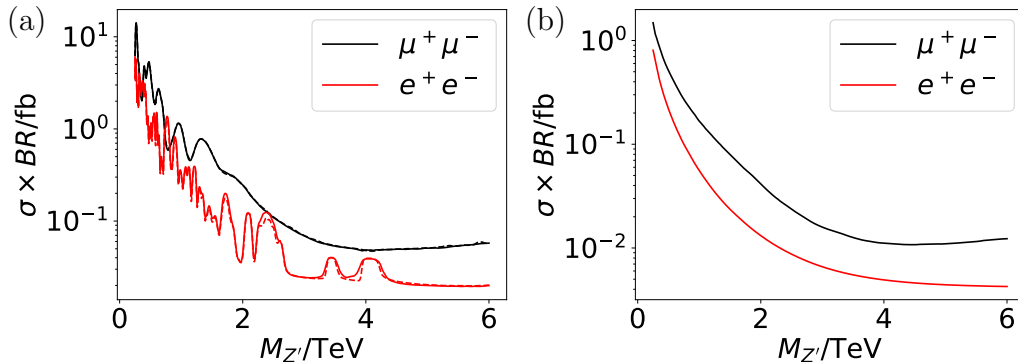


Figure 3: ATLAS bounds from resonant di-lepton searches. (a) Validation of our interpolation: the solid lines show the 95% CL upper bound for $\Gamma/M_{Z'} = 0.012$ observed by ATLAS [13] whereas our interpolations from (5) are shown by dashed curves. Where a dashed curve is not visible, it coincides with a solid one, indicating an excellent approximation. (b) Estimated HL-LHC sensitivity for a narrow Z' .

fb^{-1} . It is convenient for us to estimate the sensitivity assuming the same centre-of-mass energy as Run I (13 TeV); although the energy and future running schedule is unknown, it is likely to be at a slightly higher energy (indeed, the latest LHC run has been recording pp collisions at 13.6 TeV). We may expect higher centre-of-mass energies to have higher sensitivities to TeV-scale heavy resonant states, since the production cross-sections increase but the backgrounds are low. We may therefore expect the HL-LHC sensitivity to be similar but slightly higher than a prediction based on a slightly lower energy. Given the large uncertainty in the final integrated luminosity, we deem our rough estimate sufficient. When backgrounds are low as is the case for larger values of $M_{Z'}$, the sensitivity scales as the square root of the expected number of signal events $\sqrt{S} \propto \sqrt{\mathcal{L}}$. Even when the expected number of background events B is *not* low, the sensitivity of a search roughly scales as S/\sqrt{B} and since both S and B are proportional to the integrated luminosity collected \mathcal{L} , we still expect the sensitivity to scale proportional to $\sqrt{\mathcal{L}}$. As pointed out in Ref. [17], such arguments can lead to an underestimate in the sensitivity enhancement due to various improvements in analyses that become possible because of the opening up of new exclusive phase space regions. We shall nevertheless project the expected sensitivity from the LHC Run II analysis at integrated luminosity \mathcal{L}_0 assuming an enhancement by a factor $\sqrt{\mathcal{L}/\mathcal{L}_0}$, bearing in mind that it is a rather conservative *underestimate*. We show the resulting estimate in Fig. 3b for a narrow Z' by scaling the

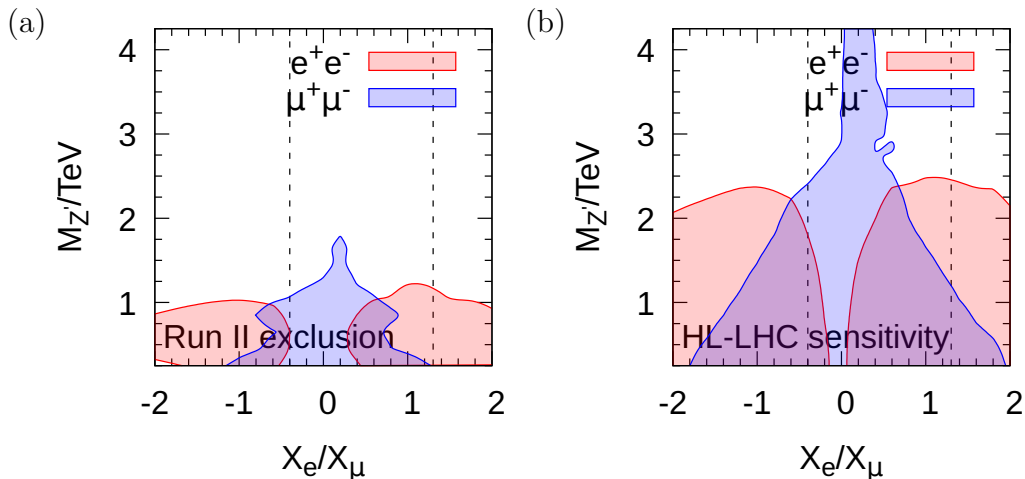


Figure 4: ATLAS di-lepton searches for Z' models that fit $b \rightarrow sl^+l^-$ data, for $X_\mu = 10$. X_e/X_μ is the ratio of the charges of first family leptons to that of second family leptons under the additional spontaneously broken $U(1)_X$ gauge symmetry. At every point, θ_{sb} and $g_{Z'}$ were profiled by the fit to flavour and LEP-2 data as in Ref. [8]. The 95% best-fit region of X_e/X_μ is the region between the two dashed lines. In (a), the filled regions are excluded at the 95% CL by the LHC Run II ATLAS di-lepton search for the channel indicated in the legend. In (b), the filled regions denote our estimate of the HL-LHC sensitivity.

ATLAS estimates of its own sensitivity in LHC Run II [13]. In the following sensitivity estimates for our model line, we shall use the interpolation (5) in z , everywhere substituting expected sensitivities for s .

CMS has performed similar searches to the ATLAS ones described above [18]. The resulting bounds on Z' bosons are similar to those of ATLAS and we therefore expect similar exclusion limits⁴.

In Fig. 3a, we display the bounds from the Run II ATLAS search. We see that, depending upon the ratio⁵ X_e/X_μ , the 95% lower CL limit on $M_{Z'}$ lies between 0.8 – 1.8 TeV. Fig. 1a shows that $M_{Z'}$ has a maximum of between 10 and 35 TeV, depending upon X_e/X_μ . We deduce that the direct search

⁴A CMS analysis [?] examines di-muon final states associated with b -jets, which will also provide constraints on parameter space via the associated $gb \rightarrow Z'b$ production channel.

⁵For values of $|X_\mu|$ smaller than 10, $g_{Z'}$ becomes larger at the best-fit point, resulting in a larger Z' production cross-section, as in (2). The pertinent Z' branching ratios would change according to Table 1 and (4): one acquires smaller di-lepton branching ratios for smaller X_μ , X_e . The sensitivity would thus be modified by the two competing effects of cross-section versus branching ratio.

rules out less than a fifth of this parameter space. In terms of $M_{Z'}$, Fig. 3b shows that the HL-LHC is expected to more than double the LHC reach, whichever the value of $X_e/X_\mu \in [-2, 2]$. Unless the Z' of the model were to be discovered at the HL-LHC, a more powerful collider (e.g. a 100 TeV pp collider) would be needed to cover all of the remaining parameter space.

Acknowledgements

This work has been partially supported by STFC consolidated grants ST/T000694/1 and ST/X000664/1. We thank the Cambridge Pheno Working Group for helpful discussions and the Glasgow Particle Physics Theory group for hospitality enjoyed while part of this work was carried out.

References

- [1] N. Gubernari, M. Reboud, D. van Dyk, J. Virto, Improved theory predictions and global analysis of exclusive $b \rightarrow s\mu^+\mu^-$ processes, JHEP 09 (2022) 133. [arXiv:2206.03797](#), [doi:10.1007/JHEP09\(2022\)133](#).
- [2] R. Aaij, et al., Branching Fraction Measurements of the Rare $B_s^0 \rightarrow \phi\mu^+\mu^-$ and $B_s^0 \rightarrow f_2'(1525)\mu^+\mu^-$ Decays, Phys. Rev. Lett. 127 (15) (2021) 151801. [arXiv:2105.14007](#), [doi:10.1103/PhysRevLett.127.151801](#).
- [3] R. Aaij, et al., Angular analysis of the $B^0 \rightarrow K^{*0}\mu^+\mu^-$ decay using 3 fb^{-1} of integrated luminosity, JHEP 02 (2016) 104. [arXiv:1512.04442](#), [doi:10.1007/JHEP02\(2016\)104](#).
- [4] M. Aaboud, et al., Angular analysis of $B_d^0 \rightarrow K^*\mu^+\mu^-$ decays in pp collisions at $\sqrt{s} = 8$ TeV with the ATLAS detector, JHEP 10 (2018) 047. [arXiv:1805.04000](#), [doi:10.1007/JHEP10\(2018\)047](#).
- [5] A. M. Sirunyan, et al., Measurement of angular parameters from the decay $B^0 \rightarrow K^{*0}\mu^+\mu^-$ in proton-proton collisions at $\sqrt{s} = 8$ TeV, Phys. Lett. B 781 (2018) 517–541. [arXiv:1710.02846](#), [doi:10.1016/j.physletb.2018.04.030](#).
- [6] W. G. Parrott, C. Bouchard, C. T. H. Davies, Standard Model predictions for $B \rightarrow K\ell^+\ell^-$, $B \rightarrow K\ell^1\ell^2$ and $B \rightarrow K\nu\bar{\nu}$ using form factors from $N_f=2+1+1$ lattice QCD, Phys. Rev. D 107 (1) (2023) 014511,

- [Erratum: Phys.Rev.D 107, 119903 (2023)]. [arXiv:2207.13371](#), [doi:10.1103/PhysRevD.107.014511](#).
- [7] R. Aaij, et al., Test of lepton universality in $b \rightarrow s\ell^+\ell^-$ decays, Phys. Rev. Lett. 131 (5) (2023) 051803. [arXiv:2212.09152](#), [doi:10.1103/PhysRevLett.131.051803](#).
- [8] B. Allanach, A. Mullin, Plan B: new Z' models for $b \rightarrow s\ell^+\ell^-$ anomalies, JHEP 09 (2023) 173. [arXiv:2306.08669](#), [doi:10.1007/JHEP09\(2023\)173](#).
- [9] C. Bonilla, T. Modak, R. Srivastava, J. W. F. Valle, $U(1)_{B_3-3L_\mu}$ gauge symmetry as a simple description of $b \rightarrow s$ anomalies, Phys. Rev. D 98 (9) (2018) 095002. [arXiv:1705.00915](#), [doi:10.1103/PhysRevD.98.095002](#).
- [10] R. Alonso, P. Cox, C. Han, T. T. Yanagida, Flavoured $B - L$ local symmetry and anomalous rare B decays, Phys. Lett. B 774 (2017) 643–648. [arXiv:1705.03858](#), [doi:10.1016/j.physletb.2017.10.027](#).
- [11] B. C. Allanach, $U(1)_{B_3-L_2}$ explanation of the neutral current B -anomalies, Eur. Phys. J. C 81 (1) (2021) 56, [Erratum: Eur.Phys.J.C 81, 321 (2021)]. [arXiv:2009.02197](#), [doi:10.1140/epjc/s10052-021-08855-w](#).
- [12] A. Greljo, J. Salko, A. Smolkovič, P. Stangl, Rare b decays meet high-mass Drell-Yan, JHEP 05 (2023) 087. [arXiv:2212.10497](#), [doi:10.1007/JHEP05\(2023\)087](#).
- [13] G. Aad, et al., Search for high-mass dilepton resonances using 139 fb^{-1} of pp collision data collected at $\sqrt{s} = 13 \text{ TeV}$ with the ATLAS detector, Phys. Lett. B 796 (2019) 68–87. [arXiv:1903.06248](#), [doi:10.1016/j.physletb.2019.07.016](#).
- [14] B. C. Allanach, J. M. Butterworth, T. Corbett, Collider constraints on Z' models for neutral current B -anomalies, JHEP 08 (2019) 106. [arXiv:1904.10954](#), [doi:10.1007/JHEP08\(2019\)106](#).
- [15] J. Alwall, R. Frederix, S. Frixione, V. Hirschi, F. Maltoni, O. Mattelaer, H. S. Shao, T. Stelzer, P. Torrielli, M. Zaro, The automated computation of tree-level and next-to-leading order differential cross sections,

- and their matching to parton shower simulations, JHEP 07 (2014) 079. [arXiv:1405.0301](#), [doi:10.1007/JHEP07\(2014\)079](#).
- [16] C. Degrande, C. Duhr, B. Fuks, D. Grellscheid, O. Mattelaer, T. Reiter, UFO - The Universal FeynRules Output, Comput. Phys. Commun. 183 (2012) 1201–1214. [arXiv:1108.2040](#), [doi:10.1016/j.cpc.2012.01.022](#).
- [17] A. Belvedere, C. Englert, R. Kogler, M. Spannowsky, Dispelling the \sqrt{L} myth for the High-Luminosity LHC (2 2024). [arXiv:2402.07985](#).
- [18] A. M. Sirunyan, et al., Search for resonant and nonresonant new phenomena in high-mass dilepton final states at $\sqrt{s} = 13$ TeV, JHEP 07 (2021) 208. [arXiv:2103.02708](#), [doi:10.1007/JHEP07\(2021\)208](#).